NASA/CR-1999-209517
ICASE Report No. 99-33

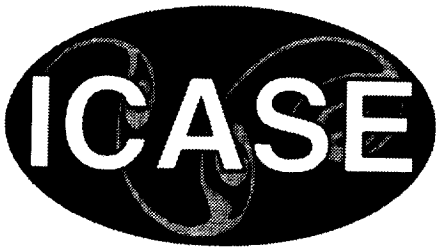

Streamwise Vorticity Generation in Laminar and Turbulent Jets

Ayodeji O. Demuren
Old Dominion University, Norfolk, Virginia
and
ICASE, Hampton, Virginia

Robert V. Wilson
The University of Iowa, Iowa City, Iowa

Institute for Computer Applications in Science and Engineering
NASA Langley Research Center
Hampton, VA

Operated by Universities Space Research Association

National Aeronautics and
Space Administration

Langley Research Center
Hampton, Virginia 23681-2199

Prepared for Langley Research Center under
Contracts NAS1-19480 and NAS1-97046

August 1999

Available from the following:

NASA Center for AeroSpace Information (CASI)
7121 Standard Drive
Hanover, MD 21076-1320
(301) 621-0390

National Technical Information Service (NTIS)
5285 Port Royal Road
Springfield, VA 22161-2171
(703) 487-4650

STREAMWISE VORTICITY GENERATION IN LAMINAR AND TURBULENT JETS

AYODEJI O. DEMUREN* AND ROBERT V. WILSON†

Abstract. Complex streamwise vorticity fields are observed in the evolution of non-circular jets. Generation mechanisms are investigated via Reynolds-averaged (RANS), large-eddy (LES) and direct numerical (DNS) simulations of laminar and turbulent rectangular jets. Complex vortex interactions are found in DNS of laminar jets, but axis-switching is observed only when a single instability mode is present in the incoming mixing layer. With several modes present, the structures are not coherent and no axis-switching occurs. RANS computations also produce no axis-switching. On the other hand, LES of high Reynolds number turbulent jets produce axis-switching even for cases with several instability modes in the mixing layer. Analysis of the source terms of the mean streamwise vorticity equation through post-processing of the instantaneous results shows that complex interactions of gradients of the normal and shear Reynolds stresses are responsible for the generation of streamwise vorticity which leads to axis-switching. RANS computations confirm these results. $k-\epsilon$ turbulence model computations fail to reproduce the phenomenon, whereas algebraic Reynolds stress model (ASM) computations, in which the secondary normal and shear stresses are computed explicitly, succeeded in reproducing the phenomenon accurately.

Key words. jets, DNS, LES, Navier-Stokes, turbulence modeling

Subject classification. Fluid Mechanics

1. Introduction. Experiments ([3, 4]) have shown that three-dimensional (3-D) jets can be used to enhance mixing and entrainment rates in comparison to axi-symmetric jets. A fundamental understanding of the dynamics of complex, turbulent jets is required for their prediction and control.

Zaman [7] used streamwise and azimuthal vorticity dynamics to explain the presence or absence of axis-switching in experimental measurements of 3:1 aspect ratio rectangular jets with different initial conditions. This study showed that the presence of streamwise vorticity pairs with outflow rotation (pumping fluid from the core to the ambient perpendicular to the major axis plane) produced axis switching while pairs with the opposite sense of rotation did not. However, in jets with no streamwise vorticity at discharge some other mechanism must originate it. Hussain and Husain [2] have explained that vortex self-induction which is an inviscid mechanism could be responsible. In the current study, numerical simulations of laminar and turbulent rectangular jets are performed to investigate the origin of streamwise vorticity and the mechanism for axis-switching through direct computations and analysis of terms in the streamwise vorticity equation.

2. Mathematical Formulation. The partial differential equations governing the incompressible jet fluid flow are variants of the Navier-Stokes equations which can be written in Cartesian tensor form, for dimensionless variables as:

$$\frac{\partial \overline{u}_i}{\partial t} + \overline{u}_j \frac{\partial \overline{u}_i}{\partial x_j} = -\frac{\partial \overline{P}}{\partial x_i} + \frac{1}{Re_D} \frac{\partial^2 \overline{u}_i}{\partial x_j \partial x_j} - \frac{\partial \tau_{ij}}{\partial x_j} \tag{2.1}$$

*Department of Mechanical Engineering, Old Dominion University, Norfolk, VA 23529 (email: demuren@mem.odu.edu). This research was supported by the National Aeronautics and Space Administration under NASA Contract Nos. NAS1-19480 and NAS1-97046 while the first author was in residence at the Institute for Computer Applications in Science and Engineering (ICASE), NASA Langley Research Center, Hampton, VA 23681.

†Iowa Institute of Hydraulic Research, The University of Iowa, Iowa City, IA 52242.

and

$$\frac{\partial \overline{u}_i}{\partial x_i} = 0 \tag{2.2}$$

where $\overline{u}_i$ represents components of the velocity which are resolved in the computations, and $\tau_{ij} = \overline{u_i u_j} - \overline{u}_i \overline{u}_j$ is the Reynolds stress which must be modeled in terms of the resolved velocity field. At low Reynolds numbers, all scales of the velocity are resolved, therefore no modeling is required and the Reynolds stress is zero. Two variants are considered for high Reynolds number jet flows.

In the LES formulation, the larger scales of the flow are resolved, and the smaller scales are modeled in terms of sub-grid scale (SGS) Reynolds stress. The Smagorinsky eddy-viscosity model is utilized in the present study to approximate the SGS Reynolds stress as:

$$\tau_{ij} - \frac{\delta_{ij}}{3}\tau_{kk} = -2C_S\overline{\Delta}^2|\overline{S}|\overline{S}_{ij} \tag{2.3}$$

where δ_{ij} is the Kronecker delta, $\overline{\Delta}$ is a (dimensionless) length scale associated with the grid size, $\overline{S}_{ij} = \frac{1}{2}\left(\frac{\partial \overline{u}_i}{\partial x_j} + \frac{\partial \overline{u}_j}{\partial x_i}\right)$ is the resolved strain rate tensor, and $|\overline{S}| = \sqrt{2\overline{S}_{lm}\overline{S}_{lm}}$. The model coefficient, C_S, is set to the constant value of 0.01. The budget of the time-averaged momentum equations show ([5]) that, in present model studies, magnitudes of the SGS stresses are only a small fraction of magnitudes of the resolved stresses, hence the use of a more sophisticated SGS model is unwarranted.

In the RANS formulation, only the mean flow is resolved. Both small and large scales are time-averaged, and their effects are modeled via the turbulent Reynolds stress. Two turbulence models are considered for approximating the Reynolds stress; the $k-\epsilon$ model which is based on a Boussinesq eddy viscosity hypothesis, similar to Eq. 2.3, and an algebraic Reynolds stress model (ASM), which is the simplest form for a second-moment turbulence closure. In the former, the Reynolds stress is calculated from:

$$\tau_{ij} - \frac{\delta_{ij}}{3}\tau_{kk} = -\nu_t \overline{S}_{ij} \tag{2.4}$$

In the latter, it can be shown ([1]) that the Reynolds stress has two parts; a linear part with exactly the same form as Eq. 2.4, and a non-linear part. Thus,

$$\tau_{ij} = \tau^*_{ij} + \tau'_{ij} \tag{2.5}$$

where τ^*_{ij} is given by Eq. 2.4 and, for the secondary Reynolds stress components, which are critical for the generation of streamwise vorticity, τ'_{ij} has the form:

$$\tau'_{ij} = k\left[\frac{2}{3}\alpha_1\delta_{ij} - \alpha_2 T^2 \frac{\partial U_1}{\partial x_i}\frac{\partial U_1}{\partial x_j}\right] \tag{2.6}$$

In Eq. 2.6, $T = k/\epsilon$ is the turbulent time scale, and α_1 and α_2 are model coefficients. Hence, the second term of this equation, which is non-linear in T also represents a ratio of turbulent to mean time scales. In addition, it embodies the anisotropy of the turbulent field. At low Reynolds numbers, the ratio will be small, and the contribution of the term will tend to zero. This ASM, though highly simplified was shown by Demuren and Rodi [1] to be capable of successfully predicting turbulence-driven secondary flow in non-circular ducts.

For DNS or LES, Eq. 2.1 is discretized temporally with explicit Runge-Kutta (RK) schemes and spatially with implicit compact finite difference schemes. Detailed descriptions are given in Wilson [5]. For RANS, the commercial code CFX-TASCflow, which uses second-order spatial discretization, is utilized.

3. Model Problems. Spatial simulations of jet flows are performed in this study in which a fixed region of the flow is computed and disturbances grow in the streamwise direction. Rectangular jets are simulated which have a nominal aspect ratio of 2:1. Reynolds numbers based on the core velocity and the equivalent diameter (D) are 750 for laminar cases and 75,000 for turbulent cases. Details of the DNS and LES can be found in Wilson and Demuren [6]. Typical computations utilized (129 x 129 x 129) grid nodes for a domain size of (12 x 10 x 10) and required several hours of CPU time on the CRAY C-90 supercomputer. The RANS simulations were performed for a one-quarter segment, taking advantage of symmetry conditions. For this quarter-segment, the domain size relative to the jet diameter was (12 x 3 x 3) and the grid distribution was (80 x 40 x 40). Convergence was obtained in about 200 iterations which required about 6 hours of CPU time on a SUN ULTRA 10/360 workstation.

4. Results and Discussion. Figure 4.1 shows contours of the instantaneous total vorticity for rectangular jets at low Reynolds number (=750) along major and minor axes, respectively. The jet in the top frames (a, b) has fundamental mode instability imposed in the mixing layer at its inlet. This would be typical of a jet issuing from a pipe with a laminar boundary layer. The lower jet (c, d) has broad mode instabilities imposed in the mixing layer at its inlet, which would be typical of a jet issuing from a pipe with a turbulent boundary layer. The former shows well-organized structures, which by the end of the simulation at 10 diameters had led to a shrinking of the jet in the major-axis plane and an expansion in the minor axis plane. In the latter, the structures are not so well-organized and no axis-switching can be discerned. This result would also be typical of a natural unforced jet. Time-averaged results of the streamwise vorticity and velocity, shown in Figure 4.2 confirm that, in the mean, no axis-switching occurs. The structures are organized, in the mean, but they lead to a gradual evolution of the jet cross-section from rectangular at inlet to circular in the far-field. The streamwise vorticity field is such that would produce this gradual transition. Therefore, at low Reynolds number, a natural rectangular jet or one with a broad mode of instabilities in its mixing layer would not experience the phenomenon of axis-switching, whereas a rectangular jet with a fundamental instability mode forcing would. It was also shown in Wilson and Demuren [6] that with the addition of the sub-harmonic mode the tendency is towards jet bifurcation. Figure 4.3 shows the instantaneous total and streamwise vorticity from the LES of rectangular jets at high Reynolds number (=75,000), with broad-mode instabilities, along minor and major axes, respectively. There is no discernible streamwise vorticity in the first 2 diameters, and the evolution trends are quite different from those of the laminar jet: there is expansion in the minor-axis plane and contraction in the major-axis plane. Corresponding time-averaged results of the streamwise vorticity and velocity, shown in Figure 4.4. So what is the origin of axis-switching, and in what flow situations would it be expected to occur?

4.1. Mechanism for Streamwise Vorticity Generation. The mechanism for streamwise vorticity generation can be examined by considering the time-averaged streamwise vorticity equation. Following Demuren and Rodi [1], the streamwise vorticity equation has the form:

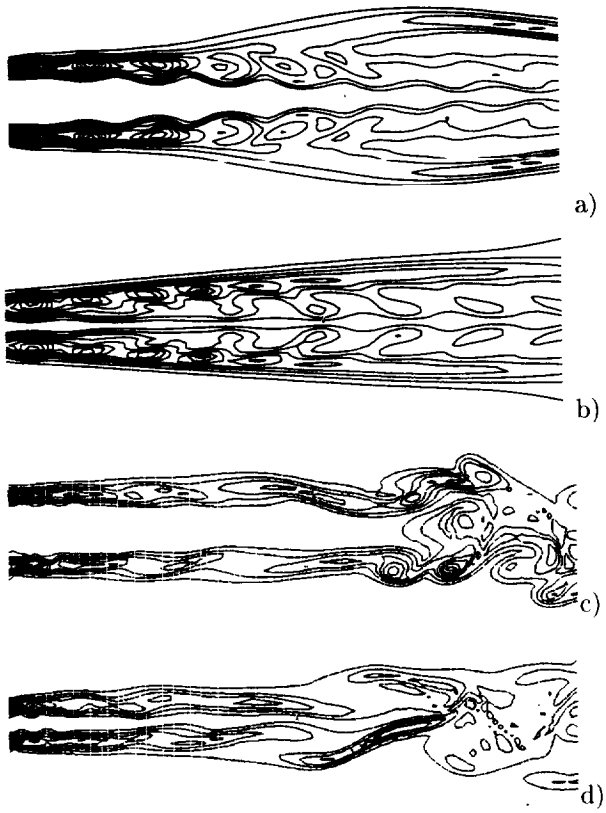

FIG. 4.1. *Instantaneous total vorticity for DNS of rectangular jet at* $Re = 750$, *with (a, b) fundamental and (c, d) broad mode instabilities.*

$$(4.1)\qquad \underbrace{U_i \frac{\partial \omega_1}{\partial x_i}}_{A_1} \underbrace{-\omega_i \frac{\partial U_1}{\partial x_i}}_{A_2} = \underbrace{\frac{\partial}{\partial x_1}\left(\frac{\partial \overline{u_1 u_2}}{\partial x_3} - \frac{\partial \overline{u_1 u_3}}{\partial x_2}\right)}_{A_3} + \underbrace{\frac{\partial^2}{\partial x_2 \partial x_3}\left(\overline{u_3^2} - \overline{u_2^2}\right)}_{A_4}$$
$$\underbrace{-\left(\frac{\partial^2}{\partial x_3^2} - \frac{\partial^2}{\partial x_2^2}\right)\overline{u_2 u_3}}_{A_5} + \underbrace{\frac{1}{Re_D}\left(\frac{\partial^2 \omega_1}{\partial x_j \partial x_j}\right)}_{A_6}.$$

The components of the vorticity vector are given by:

$$\omega_1 = \frac{\partial U_2}{\partial x_3} - \frac{\partial U_3}{\partial x_2},\ \omega_2 = \frac{\partial U_1}{\partial x_3} - \frac{\partial U_3}{\partial x_1},\ \omega_3 = \frac{\partial U_2}{\partial x_1} - \frac{\partial U_1}{\partial x_2}.$$

The A_1 terms represent the convection of streamwise vorticity by the mean velocity while the A_2 terms represent the tilting and stretching of the vorticity vector by gradients of the mean velocity. Terms A_3, A_4, and A_5 contain the turbulent stresses and act to produce or destroy streamwise vorticity. In particular, terms A_4 and A_5 contain the effect of the turbulent normal and shear stresses, respectively. The diffusion of streamwise vorticity is given by the terms, A_6.

The generation of streamwise vorticity through vortex stretching and tilting (terms A_2) is known as secondary motion of Prandtl's first kind. This is an inviscid mechanism which may be present in laminar as well as turbulent flows. Generation of streamwise vorticity by gradients of the turbulent stresses (terms A_3, A_4, and A_5) is known as secondary motion of Prandtl's second kind. Since there is no mean streamwise

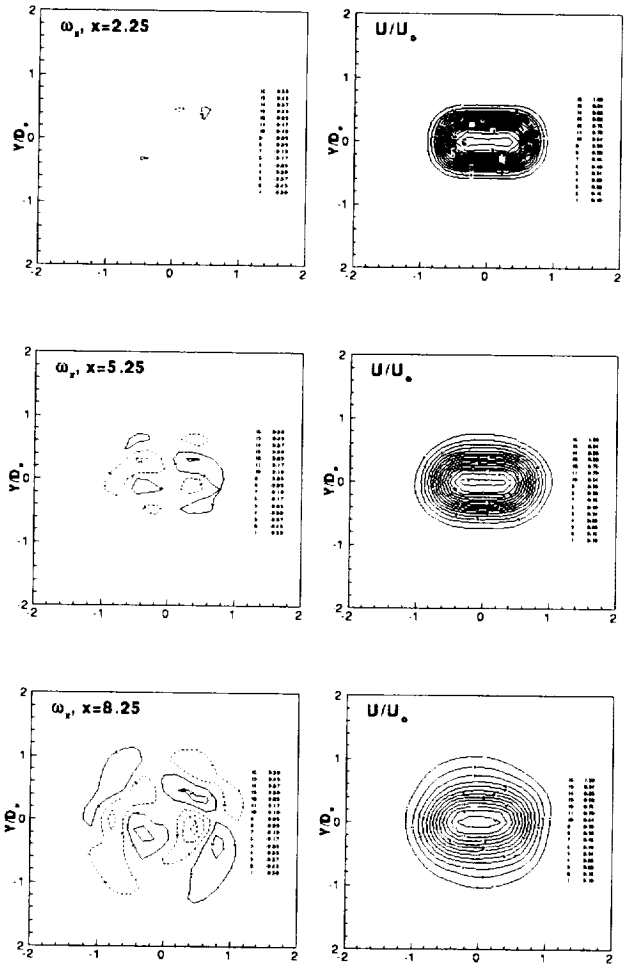

FIG. 4.2. *Cross-sectional contours of mean streamwise vorticity and velocity for DNS of rectangular jet at* $Re = 750$ *with broad mode instabilities.*

vorticity imposed at the inflow of the current simulations, its generation downstream of the inflow can only be explained by tilting and stretching of the azimuthal vorticity and/or by gradients of the turbulent normal and shear stresses.

The terms of the mean streamwise vorticity equation were computed by post-processing the instantaneous results from the DNS and LES of the spatially-developing rectangular jet with broad mode forcing. An examination of these can illuminate the origin of streamwise vorticity in these jets. The results show that the streamwise vorticity component in the first two diameters is several orders of magnitude smaller than the azimuthal component at the inflow. Streamwise vorticity undergoes rapid growth in the region $2.5 < x/D < 4$.

In the presence of fundamental mode instability, rollers are formed in the mixing layer of the jet, which would be rectangular vortex rings in the case of a rectangular jet. But from the Biot-Savart law, vortex rings have induced velocities which are proportional to their curvature. Hence, in the corners or along the minor-axis sides, the induced velocities would be larger than those along the major-axis sides. The differential induced velocity lead to deformation of the vortex rings and hence the jet, shown in Figure 4.1.

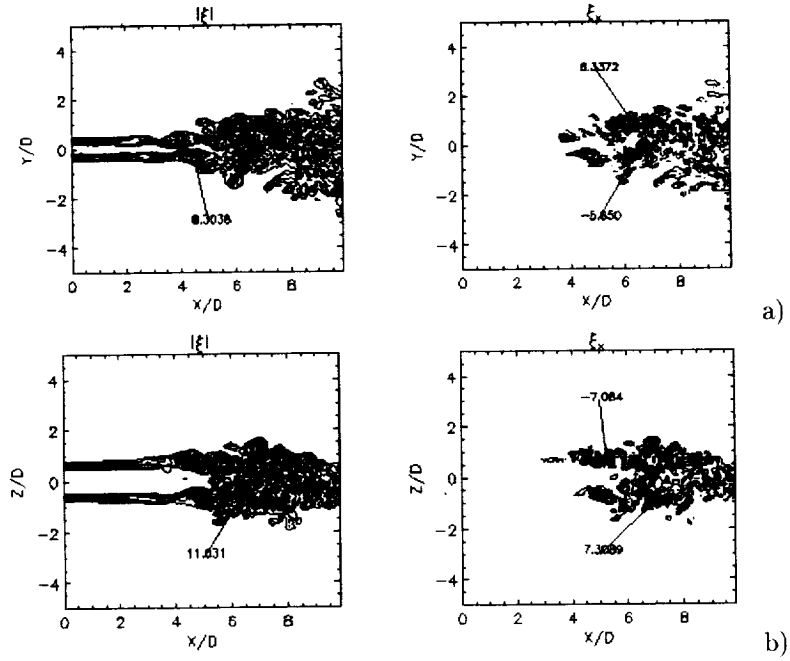

FIG. 4.3. *Instantaneous total and streamwise vorticity for LES of rectangular jet at* $Re = 75,000$ *with broad mode instabilities a) minor axis and b) major axis.*

The mechanism is inviscid and the jet deformation would proceed in this way, whether the jet is laminar or turbulent, so long as the vortex rings represent the dominant structure in the jet. This has been widely observed in the literature, and indeed, in many experimental and numerical studies, very strong forcing at the fundamental mode is applied not only to the mixing layer, but also to the whole jet. The consequence is that the jet evolution is largely governed by this discrete-mode forcing.

In natural jets or jets with broad-mode forcing, organized vortex rings, if present at all, play only a minor role. In the laminar jet, the A_2 term is dominant and shows the gradual transfer of vorticity from the azimuthal components to the streamwise component. This process continues to increase the streamwise component even beyond $x/D = 8.25$. The jet shape distorts from its initial rectangular to a circular one in the process. No axis-switching occurs in this case. In the turbulent jet, on the other hand, streamwise vorticity growth is initially due to the A_2 and A_4 terms. The A_5 term quickly builds and surpasses the A_2 term, which subsequently stagnates and decays. Both the A_4 and A_5 terms grow to reach their maximum value before the end of the potential core.

To obtain a global picture of the interaction of the source terms of the streamwise vorticity equation, detailed cross-sectional plots are required (not shown here) to analyze the distribution of the source terms within the cross-sectional plane and to explain the generation of the streamwise vorticity and axis switching mechanism. Cross-sectional contours of the A_2, A_4, A_5, and the $A_4 + A_5$ terms, at $x/D = 3$, along with the mean streamwise vorticity and velocity show that eight pairs of streamwise vortices are present and their locations and signs are consistent with that of the $A_4 + A_5$ term. Hence, it is shown that gradients of the difference of the turbulent normal stresses are responsible for the initial generation of streamwise vorticity. Contour patterns of streamwise vorticity and of the A_4 term show little bias towards the major or minor axis planes, while contours of the $A_4 + A_5$ term begin to show an anisotropic pattern. Further downstream at $x/D = 3.75$, contours of streamwise vorticity reveal that the vortex pairs orientated about

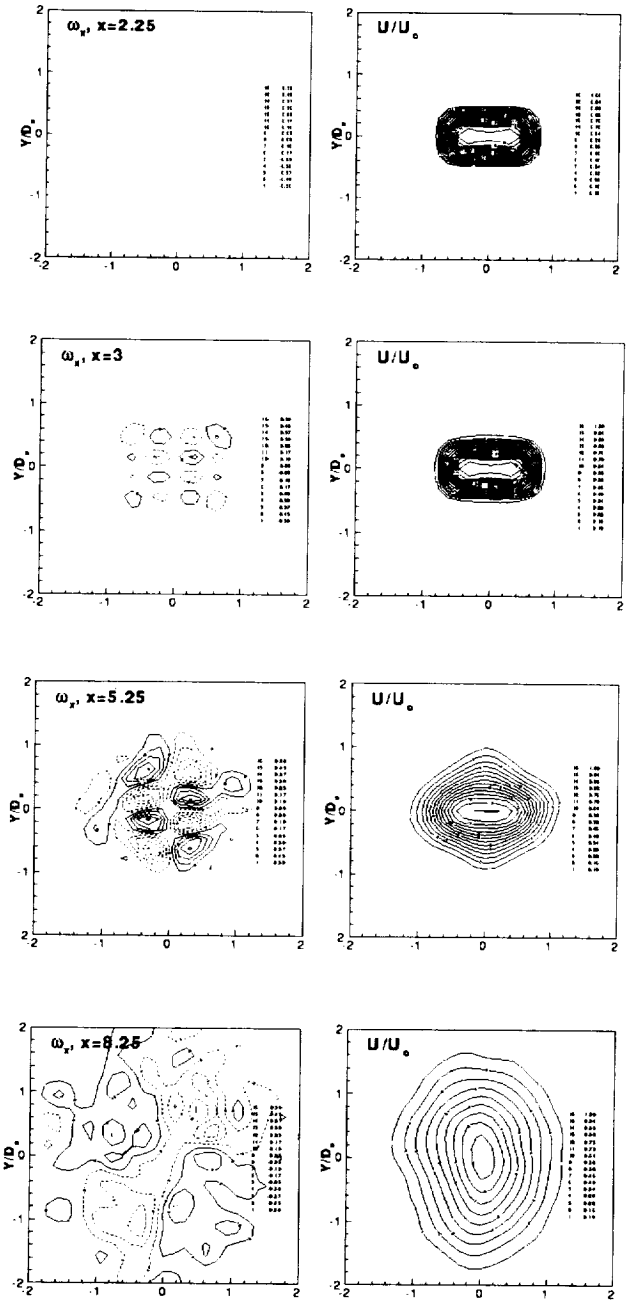

FIG. 4.4. *Cross-sectional contours of mean streamwise vorticity and velocity for LES of rectangular jet at* $Re = 75,000$.

the minor axis plane are of greater strength than those along the major axis plane. Contours of the A_5 term show a coalescence of the like-signed contours present at $x/D = 3$ along the major axis plane, resulting in a weakening of the opposite-signed patterns of the A_4 term along the major axis plane. This is apparent from the contours of the $A_4 + A_5$ terms and explains the directional bias present in the streamwise vorticity contours. The sense of rotation of the vortex pairs about the minor axis plane is such that core velocity fluid is pumped from the jet centerline to the ambient leading to a distortion of the initially rectangular mixing layer.

The four pair of streamwise vortices oriented along the minor axis strengthen until the end of the potential core where the initially flat major axis sides develop a bulge and the corners are flattened, leading to the observed diamond shape at $x/D = 5.25$ (Figure 4.4) and the eventual switching of the major and minor axes. Comparison of the structures of the A_4, A_5 terms and the streamwise vorticity suggests that the A_4 term acts largely as a source and the A_5 term as a sink, and the difference between them produces the streamwise vorticity. The inviscid mechanism, based on the Biot-Savart law or A_2 plays no significant role. These are exactly the roles that Demuren and Rodi [1] found that the turbulent terms played in generating streamwise vorticity in non-circular ducts. This similarity suggests that RANS computations based on second-moment closure models should reproduce these effects whereas those based on Boussinesq-type eddy-viscosity models should fail.

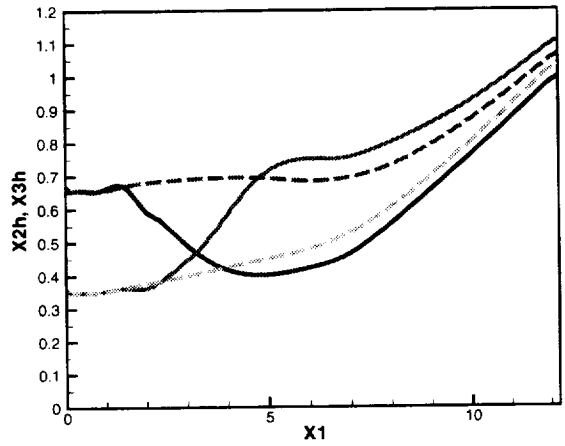

FIG. 4.5. *Jet half-widths for RANS calculation of rectangular jet at Re = 75,000; ASM - solid lines, $k-\epsilon$ - dashed lines.*

Results of RANS computations of the turbulent rectangular jet at a Reynolds number of 75,000 are presented in Figures 4.5 and 4.7. Figure 4.5 shows the growth of the jet half-widths. The ASM results exhibit growth along the minor axis and decline along the major axis, with a cross-over between the major and minor axes at x/D of 3. On the other hand, the $k-\epsilon$ model results show growth along both axes, but at a faster rate along the minor axis so that by the end of the calculation domain at x/D of 12, both widths are nearly equal. Flow patterns are shown in Figure 4.6 for three cross-stream locations, x/D of 1.25, 2.5 and 5. The $k-\epsilon$ model results show entrainment of ambient fluid from both sides and some transfer of the fluid from the narrow side to the wide side which leads to faster growth of the jet along the minor axis, and the approach towards a circular cross-section. This result mirrors that shown in Figure 4.2 for laminar rectangular jets rather than the turbulent jet ones of Figure 4.4. The ASM results show much more complex flow patterns. At x/D of 1.25, the potential core is largely undisturbed, but the mixing layer region is highly distorted. There is a strong reverse flow region, and the sense of the circulation is to move fluid from the narrow side to the wide side which produces strong distortion of the streamwise velocity contours. By 2.5 diameters, the jet shape is now highly distorted, though a potential core still exists which maintains its rectangular shape. But by 5 diameters, at the end of the potential core, the major and minor axes of the jet have switched, and there is now one major circulation which sense is to continue the axis-switching process. Figure 4.7 shows the streamwise vorticity contours. At x/D of 1.25, there are two pairs of vortices, consistent with the LES results of Figure 4.4. The vortex strength increases up to 2.5 diameters, where only one pair remains. The bulk of the jet distortion occurs in this region. By 5 diameters, the strength of the vortex

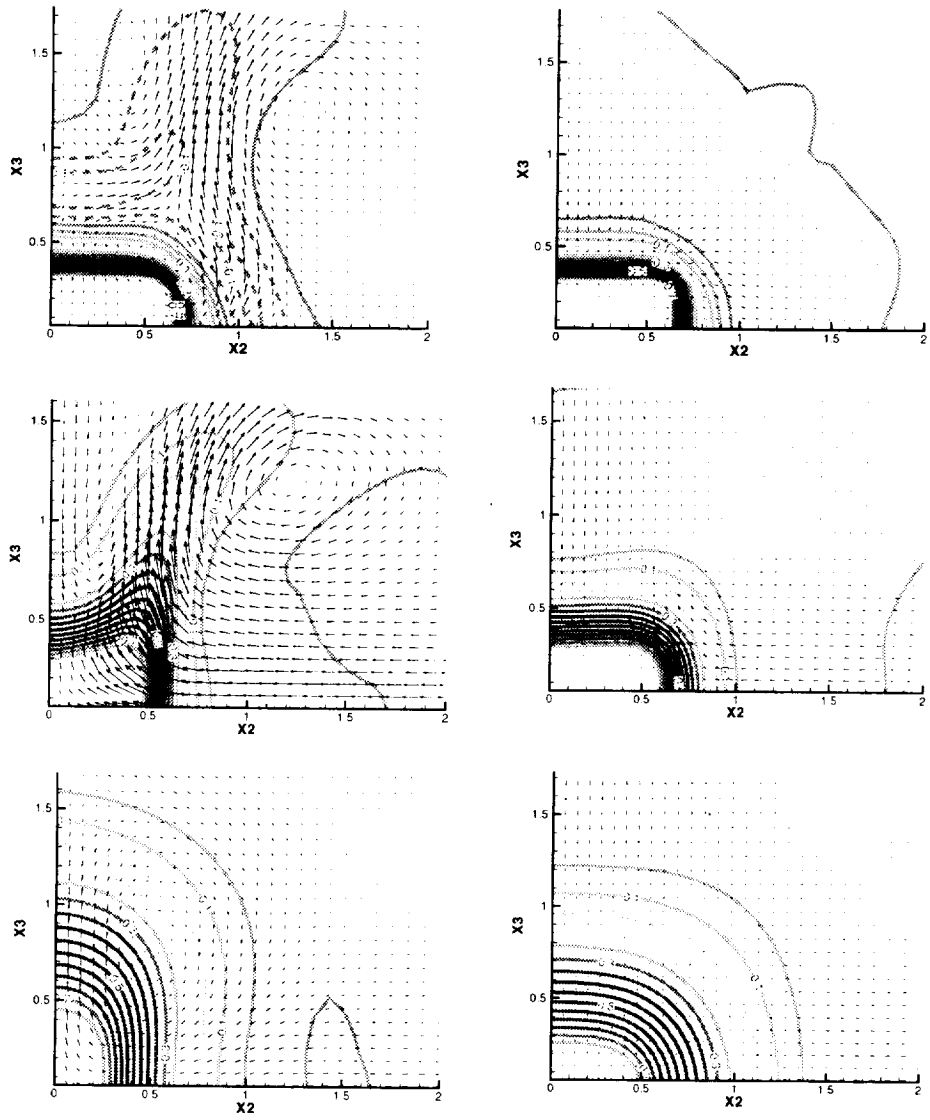

FIG. 4.6. *Mean velocity vectors and streamwise velocity contours at* $X/D = 1.25, 2.5, 5.0$, *for RANS computations of rectangular jet at* $Re = 75,000$; *ASM - left side,* $k - \epsilon$ *- right side.*

has decreased by almost one order of magnitude below the peak value. What is seen are the final stages of the axis-switching process. The LES and RANS computations with ASM show good qualitative agreement, though the vortex strengths appear to be higher and the axes appeared to switch earlier in the latter. Jet evolution has been shown in the present study, and in many experiments, to be strongly influenced by the instabilities or turbulence in the inlet mixing layer, so quantitative comparisons would require a closer match of these conditions. Furthermore, the version of second-moment closure utilized here is highly simplified and was found to over-predict secondary flow generation in some non-circular ducts, though essential features are reproduced. It was adopted here for its simplicity, as the lowest level of modeling required to confirm the explanations for the origin of mean streamwise vorticity found in the analysis of the LES results.

5. Concluding Remarks. Three-dimensional simulations of laminar and turbulent jets with rectangular cross-section were performed. At low Reynolds numbers DNS were performed, while at higher Reynolds

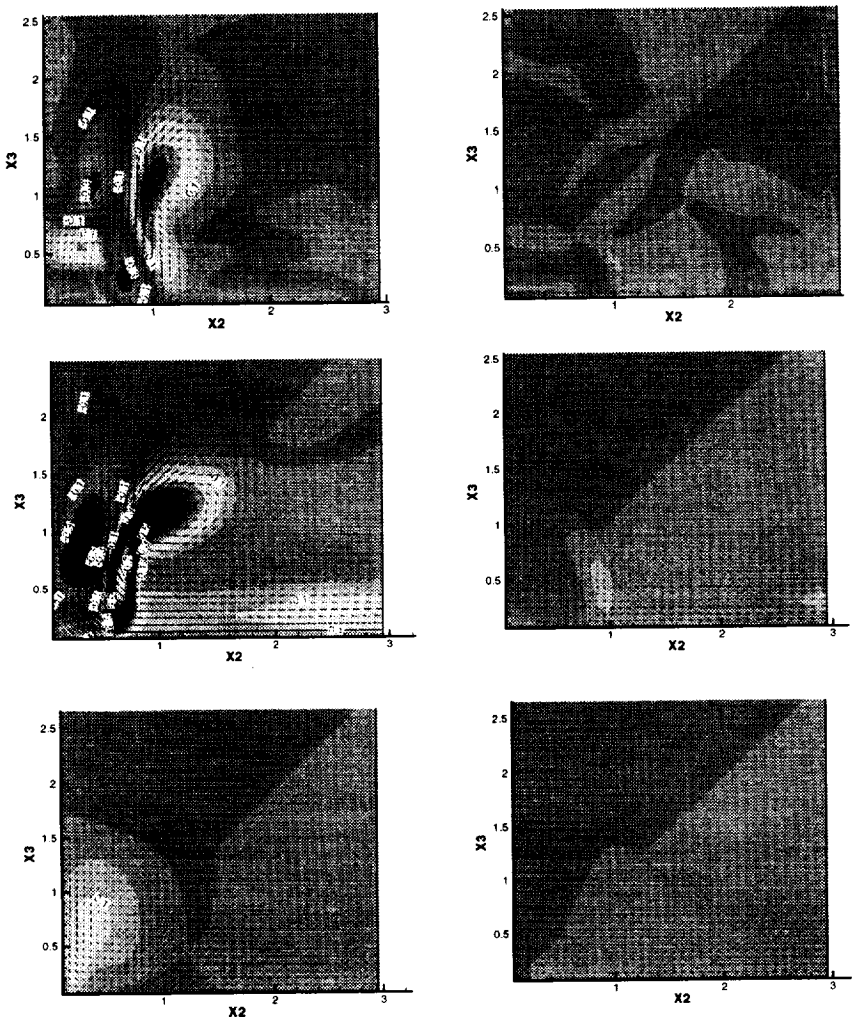

FIG. 4.7. *Mean velocity vectors and streamwise vorticity contours at* $X/D = 1.25, 2.5, 5.0$, *for RANS computations of rectangular jet at* $Re = 75,000$; *ASM - left side,* $k - \epsilon$ *- right side.*

numbers LES or RANS computations were performed. Origin of secondary flow or streamwise vorticity under different conditions of the spectral content of the initial jet mixing layer or Reynolds number are investigated through budgets of the mean streamwise vorticity derived from the DNS and LES data. Inviscid mechanisms, which can be explained by the evolution of vortex rings are responsible for the distortion of laminar jets with discrete mode forcing. Natural laminar jets evolve in an uneventful manner from rectangular to circular cross-section. In turbulent jets, streamwise vorticity is generated by terms involving derivatives of the secondary Reynolds normal and shear stresses. Inviscid mechanisms play no role. These results are confirmed by RANS computations with ASM.

REFERENCES

[1] A.O. DEMUREN AND W. RODI, *Calculation of Turbulence-driven Secondary Motion in Non-circular Ducts*, Journal of Fluid Mechanics **140** (1984), pp. 189–222.

[2] F. HUSSAIN AND H.S. HUSAIN, *Elliptic Jets. Part 1. Characteristics of Unexcited and Excited Jets*, Journal of Fluid Mechanics **208** (1989), pp. 257–320.

[3] W.R. QUINN, *On Mixing in an Elliptic Turbulent Free Jet*, Physics of Fluids. A. **1**, No. 10 (1989), pp. 1716–1722.

[4] Y. TSUCHIYA AND C. HORIKOSHI, *On the Spread of Rectangular Jets*, Experiments in Fluids **4** (1986), pp. 197–204.

[5] R.V. WILSON, *Numerical Simulation of Complex Three-dimensional Turbulent Jets*, Ph.D. Thesis, Old Dominion University, Norfolk, VA, 1996.

[6] R.V. WILSON AND A.O. DEMUREN, *Numerical Simulation of Turbulent Jets with Rectangular Cross-section*, ASME, Journal of Fluids Engineering **120** (1998), pp. 285–290.

[7] K.B.M.Q. ZAMAN, *Axis Switching and Spreading of an Asymmetric Jet: The Role of Coherent Structure Dynamics*, Journal of Fluid Mechanics **316** (1996), pp. 1–27.

REPORT DOCUMENTATION PAGE

Form Approved
OMB No. 0704-0188

1. AGENCY USE ONLY *(Leave blank)*

2. REPORT DATE
August 1999

3. REPORT TYPE AND DATES COVERED
Contractor Report

4. TITLE AND SUBTITLE
Streamwise vorticity generation in laminar and turbulent jets

5. FUNDING NUMBERS
C NAS1-19480
C NAS1-97046
WU 505-90-52-01

6. AUTHOR(S)
Ayodeji O. Demuren
Robert V. Wilson

7. PERFORMING ORGANIZATION NAME(S) AND ADDRESS(ES)
Institute for Computer Applications in Science and Engineering
Mail Stop 132C, NASA Langley Research Center
Hampton, VA 23681-2199

8. PERFORMING ORGANIZATION REPORT NUMBER
ICASE Report No. 99-33

9. SPONSORING/MONITORING AGENCY NAME(S) AND ADDRESS(ES)
National Aeronautics and Space Administration
Langley Research Center
Hampton, VA 23681-2199

10. SPONSORING/MONITORING AGENCY REPORT NUMBER
NASA/CR-1999-209517
ICASE Report No. 99-33

11. SUPPLEMENTARY NOTES
Langley Technical Monitor: Dennis M. Bushnell
Final Report
To appear in the Proceedings of ASME/JSME Fluids Engineering Conference.

12a. DISTRIBUTION/AVAILABILITY STATEMENT
Unclassified–Unlimited
Subject Category 34
Distribution: Nonstandard
Availability: NASA-CASI (301) 621-0390

12b. DISTRIBUTION CODE

13. ABSTRACT *(Maximum 200 words)*

Complex streamwise vorticity fields are observed in the evolution of non-circular jets. Generation mechanisms are investigated via Reynolds-averaged (RANS), large-eddy (LES) and direct numerical (DNS) simulations of laminar and turbulent rectangular jets. Complex vortex interactions are found in DNS of laminar jets, but axis-switching is observed only when a single instability mode is present in the incoming mixing layer. With several modes present, the structures are not coherent and no axis-switching occurs. RANS computations also produce no axis-switching. On the other hand, LES of high Reynolds number turbulent jets produce axis-switching even for cases with several instability modes in the mixing layer. Analysis of the source terms of the mean streamwise vorticity equation through post-processing of the instantaneous results shows that complex interactions of gradients of the normal and shear Reynolds stresses are responsible for the generation of streamwise vorticity which leads to axis-switching. RANS computations confirm these results. k-e turbulence model computations fail to reproduce the phenomenon, whereas algebraic Reynolds stress model (ASM) computations, in which the secondary normal and shear stresses are computed explicitly, succeeded in reproducing the phenomenon accurately.

14. SUBJECT TERMS
jets, DNS, LES, Navier-Stokes, turbulence modeling

15. NUMBER OF PAGES
14

16. PRICE CODE
A03

17. SECURITY CLASSIFICATION OF REPORT	18. SECURITY CLASSIFICATION OF THIS PAGE	19. SECURITY CLASSIFICATION OF ABSTRACT	20. LIMITATION OF ABSTRACT
Unclassified	Unclassified		